IIT BOMBAY

Quantum Chaos and Many-Body systems

by

Kartik Patekar

160260018

Project Report for
B.Tech. Project (PH 587)

Under Guidance of

Professor Gautam Mandal
Department of Theoretical Physics, Tata Institute of Fundamental Research
Professor P. Ramadevi
Department of Physics, Indian Institute of Technology Bombay

November 2019

Contents

Chapter 1

Quantum chaos in many-body systems

Quantum Chaos is simply the study of Chaotic Quantum systems. Quantum chaos reveals a significant amount of universality in the behavior of extraordinarily different physical systems.

There are three methods to characterize Quantum Chaos

- Semi-classical Methods
- Random Matrix Theory
- Out-of-Time-Order Correlators (OTOC)

Semi-classical methods involve solving the system in the classical or semi-classical limits. If this simplified system shows chaotic behavior, it is natural to expect that the original quantum system is chaotic as well. We will not proceed in this direction. We will look at Random Matrix Theory and it's importance in characterization of Chaos in the next chapter, and here instead focus on OTOCs, which have been motivated by the study of black holes and discovery of Gauge-Gravity correspondence.

In quantum systems, Chaos can be characterised by studying the growth of different time commutator of 2 rather general Hermitian operators given by $[W(t), V(0)]$. The commutator quantifies the effect of perturbation V on a later measurement of W. When be average over ensemble of initial states, it becomes necessary to use the squared commutator so that the phases do not cancel out, and hence we study the function

$$C(t) = \langle [W(t), V(0)]^\dagger [W(t), V(0)] \rangle = -\langle [W(t), V(0)]^2 \rangle \tag{1.1}$$

We will assume that V, W are simple Hermitian operators, i.e. they can be expressed as sum of terms with each term having $\mathcal{O}(1)$ degrees of freedom. Also, V, W have been shifted such that their thermal 1-point function is zero.

$C(t)$ can be easily connected to OTOC using the expansion of the commutator

$$C(t) = \langle W(t)VVW(t)\rangle + \langle VW(t)W(t)V\rangle - 2\,\mathrm{Re}\{\langle VW(t)VW(t)\rangle\} \tag{1.2}$$

where the last term is the OTOC while the first and second term are simply the thermal two point functions, which goes to $\langle V^2\rangle\langle W^2\rangle$ at large t.

If the system is chaotic, i.e. it exhibits *Butterfly effect*, then the effect of perturbation V will grow with time and the value of $C(t)$ saturates to $2\langle V^2\rangle\langle W^2\rangle$ [1]. On the other hand, for a non-chaotic systems, the operations commute at large time and the function $C(t)$ decays to zero.

One important subtlety regarding quantum chaos needs to be clarified. Since QM is a linear theory, if two states are close initially in the sense of having large inner product, they will remain close as time progresses. However, for systems having large number of degrees of freedom, orthogonal states can be physically similar. This physical similarity of the initial states can be destroyed by the time evolution in chaotic systems.

1.1 Brief overview of classical chaos

Classical chaos is a huge field in itself, and here we will only consider the properties relevant to our discussion in later sections.

We consider a classical thermal system with phase space denoted by $\boldsymbol{X} = (\boldsymbol{p}, \boldsymbol{q})$, where $\boldsymbol{p}$ and $\boldsymbol{q}$ are multidimensional momentum and coordinate vectors. In this system, we can determine the presence of Chaos through Sensitive Dependence on Initial Condition (SDIC).

Assume that we have a reference trajectory in phase space $\boldsymbol{X}(t)$ with initial conditions $\boldsymbol{X}(0) = \boldsymbol{X}_0$. If we make a small change in the initial conditions $\boldsymbol{X}_0 \to \boldsymbol{X}_0 + \delta\boldsymbol{X}_0$, the system follows a new trajectory given by $\boldsymbol{X}(t) \to \boldsymbol{X}(t) + \delta\boldsymbol{X}(t)$. For a chaotic system showing SDIC, the distance between the reference trajectory and the perturbed trajectory increases exponentially with time and this rate of increase is given by Lyapunov exponent λ_L

$$|\delta\boldsymbol{X}(t)| \sim |\delta\boldsymbol{X}_0| e^{\lambda_L t} \tag{1.3}$$

It must be noted that we actually obtain a spectrum of Lyapunov exponent depending upon the orientation of $\delta \boldsymbol{X}_0$. However, for most deviations, only the largest Lyapunov exponent is significant at large time, and unless otherwise stated, I will refer to the maximal Lyapunov exponent as the Lyapunov exponent λ_L.

The classical thermal systems exhibiting chaotic dynamics usually have two exponential behavior.

- Lyapunov behavior $\implies$ characterises SDIC
- Ruelle behavior $\implies$ characterises approach to thermal equilibrium

Since the Black holes can also be considered as thermal systems, the analogs of these two behaviors can be studied in Black hole physics.

When we consider the SDIC, we need to use squared values of deviation to avoid cancellation on averaging over initial systems and perturbations. We consider the function

$$F(t) = \left\langle \left(\frac{\partial \boldsymbol{X}(t)}{\partial \boldsymbol{X}_0} \right)^2 \right\rangle \sim \sum_k c_k e^{2\lambda_k t} \qquad \text{at large } t \tag{1.4}$$

Ruelle's behavior characterises how fast the system forgets the initial conditions and approach the thermal equilibrium. This approach is given by the 2-point function

$$G(t) = \langle X(t)X(0)\rangle_\beta - \langle X\rangle_\beta^2 \sim \sum_j b_j e^{-\mu_j t} \qquad \text{at large } t \tag{1.5}$$

At large time, the growth of function $F(t)$ is given by the maximum Lyapunov exponent λ_L and the decay of 2-point function is given by the minimum Ruelle resonance μ.

1.2 Quantum Analogs

In quantum systems, the analogs of F and G are given by the expectation value of the squared commutator and the and 2-point correlator respectively. To see the origin of the squared commutator, consider the measure of deviation given by

$$\frac{\partial q(t)}{\partial q(0)} \sim e^{\lambda_L t} \tag{1.6}$$

In quantum system, the analogous quantity to consider is the commutator obtained by replacing the classicla Poisson bracket with the commutator.

$$\frac{\partial q(t)}{\partial q(0)} = \{q(t), p(0)\} \rightarrow \frac{1}{i\hbar}[q(t), p(0)] \tag{1.7}$$

In the large N systems, we use general operators W, V instead of p, q to obtain the form of $C(t)$ as specified in equation 3.2.

$$F(t) = \left\langle \left(\frac{\partial q(t)}{\partial q(0)} \right)^2 \right\rangle \rightarrow C(t) = -\langle [W(t), V(0)]^2 \rangle \tag{1.8}$$

1.3 Behavior of $C(t)$

There are two important time scales which occurs in study of $C(t)$ for chaotic systems. [2]

- **Scrambling Time (t_*):** $C(t)$ usually starts from zero and grows. T_* is the time when $C(t)$ becomes significant.
- **Dissipation Time (t_d):** This scale characterize the exponential decay time of 2-point expectation values of type $\langle V(0)V(t)\rangle$ and also control the late time behaviour of $C(t)$.

For chaotic systems, the function $C(t)$ grows exponentially at time scales $t_d < t < t_*$ according to the largest Lyapunov exponent λ_L, i.e. $C(t) \sim e^{2\lambda_L t}$, as shown in Figure 1.1. We also have the following approximate relations [2]

$$t_* \sim \lambda_L^{-1} \log N_{dof} \quad , \quad t_d \sim \lambda_L^{-1} \tag{1.9}$$

As stated earlier, $C(t)$ saturates at large time at value $2\langle V^2\rangle\langle W^2\rangle$. For times smaller than t_d, $C(t)$ has a negligible value of order $\mathcal{O}(N_{dof}^{-1})$

1.4 Butterfly effect

In quantum system, the operator $W(t)$ is given by

$$W(t) = e^{iHt} W e^{-iHt} = \sum_{k=0}^{\infty} \frac{(-it)^k}{k!} [H, [H, ...[H, W]]] \tag{1.10}$$

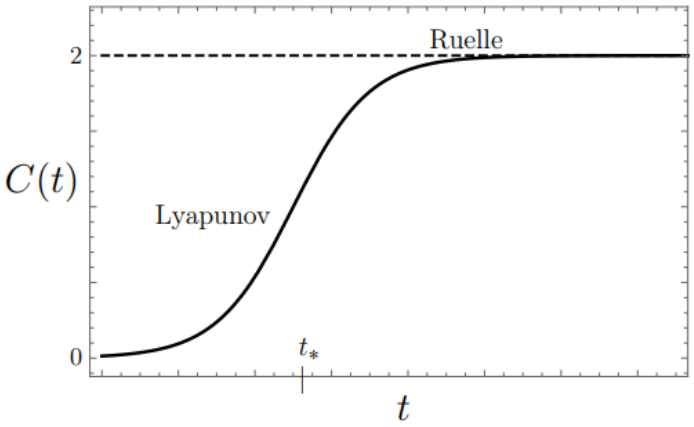

FIGURE 1.1: Typical Behavior of C(t) for chaotic systems [2]

In chaotic quantum system, operator $W(t)$ becomes more and more delocalised as time progresses. Therefore, the commutator grows exponentially in large N systems.

In we consider operators separated in space, i.e. $V(0,0$ and $W(x,t)$, for time $t > t_*$, the $C(t,x)$ actually grows as $C(t) \sim \exp\Big\{\lambda_L(t - t_* - \frac{|x|}{v_B})\Big\}$, where v_B is called the *Butterfly velocity*. This velocity characterise the growth of operator W in physical space, and bound the rate of transfer of quantum information.

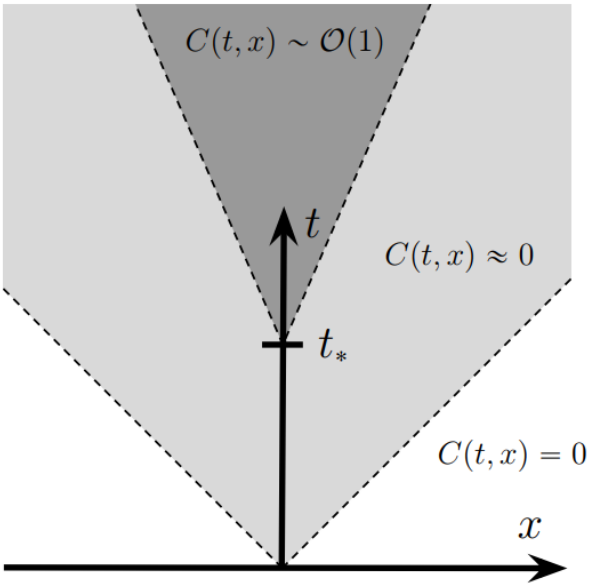

FIGURE 1.2: Butterfly effect cone [2]

For transfer of information about the perturbation, we obtain the above effective light cone where different regions are separated by different order of magnitude of $C(t)$

Chapter 2

Quantum Chaos and Random Matrix Theory

Random Matrix Theory (RMT) originated in nuclear physics as a statistical approach to understand the spectra of heavy atomic nuclei and it explained the distribution eigenvalue spacing of nuclear resonances. Motivated by the observation in SYK model [3], it is now believed that many chaotic quantum systems shares some similarities with Random Matrix Theory with regards to the Spectral statistics. Indeed, the comparison of spectral statistics of a system with that of RMT has been employed as a diagnostic of Chaos since a long time.

2.1 Introduction to RMT

For the purpose of this report, we will only consider the Gaussian Unitary Ensemble, a specific type of Random Matrix Theory. Other RMTs of interest include Gaussian Orthogonal Ensemble and Gaussian Symplectic Ensemble.

A Gaussian Unitary ensemble, specified by GUE(L, μ, σ) is an ensemble of $L \times L$ random Hermitian matrices, where each element is an independent random complex number chosen from a Gaussian distribution with mean μ and variance σ^2. Unless otherwise specified, we will be working with GUE$(L, 0, 1/\sqrt{L})$, where the variance has been chosen such that the eigenvalues do not scale with the system size. It can be shown that the energy spectrum of $GUE(L, 0, \sigma)$ lies in the range $(-2\sigma\sqrt{L}, 2\sigma\sqrt{L})$ [4].

The probability density function of matrix H in GUE is given by

$$P(H) = \exp\left\{-\frac{L}{2}\,\mathrm{Tr}\{H^2\}\right\} \tag{2.1}$$

The normalization factor has been absorbed in the measure $\mathcal{D}H$. It is obvious that GUE has $U(L)$ symmetry, and hence the integration measure is also $U(L)$ invariant, i.e. $\mathcal{D}H = \mathcal{D}(U^\dagger HU)$. Using this invariance, we can change the integral over H to integral over diagonal matrix $D = diag\{\lambda_i\}$ and unitary U according to

$$\mathcal{D}H = C|\Delta(\lambda)|^2 \mathcal{D}U \;\; \Pi_i \mathrm{d}\lambda_i \tag{2.2}$$

where the Vandermonde determinant $\Delta(\lambda)$ and the constant C are given by

$$\Delta(\lambda) = \Pi_{i<j}(\lambda_j - \lambda_i) \quad , \quad C = \frac{L^{L^2/2}}{(2\pi)^{L/2}\Pi_{p=1}^{L}(p!)} \tag{2.3}$$

We can absorb the integration over the Unitary group in the integration constant and define the joint probability distribution of eigenvalues as

$$P(\lambda_1, \lambda_1, ...\lambda_L) = C|\Delta(\lambda)|^2 \exp\left\{-\frac{L}{2}\sum_i \lambda_i^2\right\} \tag{2.4}$$

for simplicity, we define the measure over eigenvalues which absorbs their distribution as $\mathcal{D}\lambda = P(\lambda_1, ...\lambda_L)\ \Pi_i \mathrm{d}\lambda_i$. In this notation, the expectation value of the operator is given by

$$\langle O(\lambda)\rangle_{GUE} = \int \mathcal{D}\lambda O(\lambda) \tag{2.5}$$

Hence, we can obtain the spectral distribution by integrating over all but one eigenvalue

$$\rho(\lambda) = \int \mathrm{d}\lambda_1 .. \mathrm{d}\lambda_{L-1} P(\lambda_1, ..\lambda_{L-1}, \lambda) \tag{2.6}$$

In the large L limit, we obtain the Wigner semi-circle law for the distribution of eigenvalues [5]

$$\rho(\lambda) = \frac{1}{2\pi}\sqrt{4-\lambda^2} \;\; \text{as} \;\; L \to \infty \tag{2.7}$$

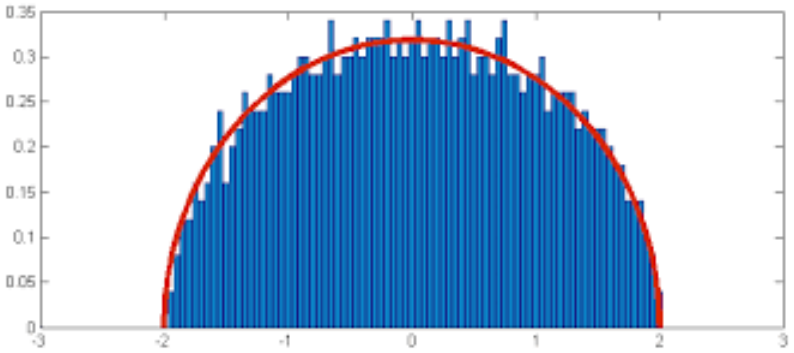

FIGURE 2.1: Wigner Semi-circle law distribution

Similarly, we can define the spectral n-point function as

$$\rho^{(n)}(\lambda_1, ...\lambda_n) = \int \mathrm{d}\lambda_{n+1}..\mathrm{d}\lambda_L P(\lambda_1, ..\lambda_{L-1}, \lambda_L) \tag{2.8}$$

According to this, the spectral 2-point function can be expressed as a sum of disconnected piece and a squared sine kernel [4] as

$$\rho^{(2)}(\lambda_1, \lambda_2) = \frac{L^2}{L(L-1)}\rho(\lambda_1)\rho(\lambda_2) - \frac{L^2}{L(L-1)}\frac{\sin^2 L(\lambda_1 - \lambda_2)}{[L\pi(\lambda_1 - \lambda_2)]^2} \tag{2.9}$$

2.2 Spectral Form Factor

For a given Hamiltonian H, the spectral form factor is defined using analytically continued partition function

$$\mathcal{R}_2^H(\beta, t) = Z(\beta, t)Z^*(\beta, t) = \mathrm{Tr}\left(e^{-\beta H - iHt}\right)\mathrm{Tr}\left(e^{-\beta H + iHt}\right) \tag{2.10}$$

In systems such as SYK model or RMT, we can average over all possible Hamiltonians to describe average spectral form factor

$$\mathcal{R}_2(\beta, t) = \langle Z(\beta, t)Z^*(\beta, t)\rangle_H \tag{2.11}$$

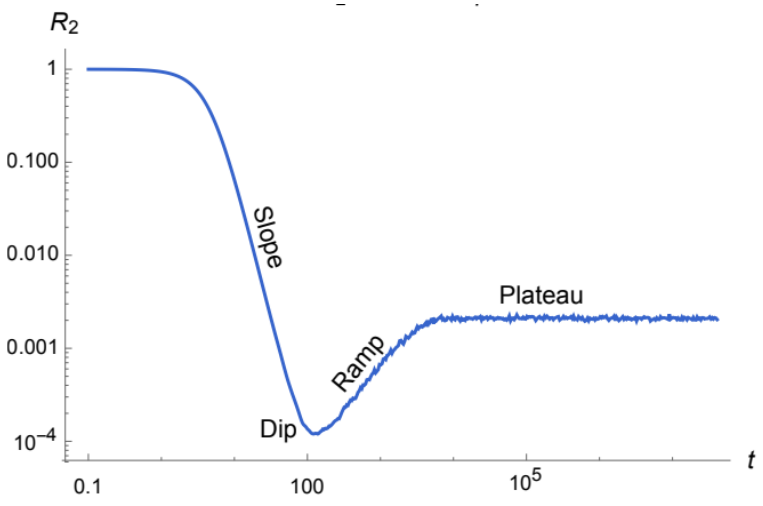

FIGURE 2.2: general behavior of spectral form factor for chaotic systems [4]

The definition of the above spectral form factor was motivated from consideration of the following 2-point correlation function

$$f_\beta(T) = \frac{1}{Z}\mathrm{Tr}\left(e^{-\beta H}O(T)e^{-\beta H}O(0)\right) = \frac{1}{Z}\sum_{n,m} e^{-(\beta+iT)E_n}e^{-(\beta-iT)E_m}|\langle n|O|m\rangle|^2 \tag{2.12}$$

Since, the squared part matrix elements vary smoothly on slightly changing the Hamiltonian, we are only interested in the oscillating part, which is

$$\mathcal{R}_2^H(\beta,t) = \sum_{n,m} e^{-(\beta+iT)E_n} e^{-(\beta-iT)E_m} \tag{2.13}$$

2.3 Spectral form factor in RMT

After taking the GUE average, the spectral form factor reduces to

$$\mathcal{R}_2(\beta,t) = \langle Z(\beta,t)Z^*(\beta,t)\rangle_{GUE} = \int \mathcal{D}\lambda \sum_{k,j} e^{-\beta(\lambda_k+\lambda_j)+i(\lambda_k-\lambda_j)t} \tag{2.14}$$

We separately study the behavior of spectral form factor in infinite T and finite T cases. Here, I will simply state the results and the detailed calculation can be found in reference [4].

2.3.1 Infinite Temperature Case

In this case, the spectral form factor reduces to

$$\mathcal{R}_2(t) = \int \mathcal{D}\lambda \sum_{k,j} e^{i(\lambda_k-\lambda_j)t} = L + L(L-1)\int \mathrm{d}\lambda_1 \mathrm{d}\lambda_2 \rho^{(2)}(\lambda_1,\lambda_2) e^{i(\lambda_1-\lambda_2)t} \tag{2.15}$$

where the first term arises from the case when $i = j$ and second term correspond to the case when $i \neq j$.

Separating $\rho^{(2)}(\lambda_1,\lambda_2)$ into connected and disconnected parts, we observe that the disconnected part is simply the Fourier transform of the spectral distribution function. The integration over the squared Sine kernel can be evaluated under the box approximation [5] to give a ramp function. The final result is

$$\mathcal{R}_2(t) = L + L^2 r_1^2(t) - L r_2(t) \tag{2.16}$$

The first contribution comes from the $i = j$ case which is constant at large t, the second contribution arises from the disconnected part and oscillates at all t while the last contribution arises from the Sine kernel and is responsible for the ramp behavior the the spectral form factor.

The functions r_1 and r_2 are given by

$$r_1(t) = \frac{J_1(2t)}{t} \tag{2.17}$$

$$r_2(t) = \begin{cases} 1 - \frac{l}{2L} & t < 2L \\ 0 & t \geq 2L \end{cases} \tag{2.18}$$

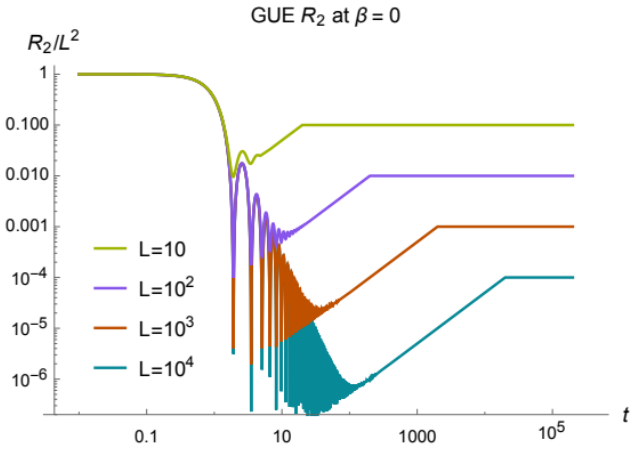

FIGURE 2.3: Spectral Form factor at infinite temperature [4]

The figure shows the results obtained by simulating the system at infinite temperature. We can distinctively identify the linear ramp, dip and plateau in the spectral form factor. The oscillations occurs due to oscillating nature of r_1 and gets smoothened out at finite temperature. The spectral form factor becomes almost constant after the plateau time t_p which can be found by function r_2 as $t_p = 2L$.

2.3.2 Finite temperature

The finite temperature spectral form factor can be written using analytical continuation of functions r_1 and r_2 as

$$\mathcal{R}_2(t) = Lr_1(2i\beta) + L^2 r_1(t + i\beta)r_1(-t + i\beta) - Lr_1(2i\beta)r_2(t) \tag{2.19}$$

This smoothens out the oscillations visible in infinite temperature case, as well as gives the correct slope of ramp as obtained in simulations.

2.4 Relation between OTOC and spectral form factor

In this section, we will relate 2-point OTOC to the spectral form factor, thus establishing the fact that both of them are more or less equivalent diagnostic of Chaos. We will be working with general hamiltonian H of dimensions $L = 2^n$. We will only consider the infinite temperature case here.

Let us consider 2-point correlation function between between a unitary operator A with time separation t. On averaging over all unitary operators

$$\frac{1}{L}\int \mathrm{d}A\langle A(0)A^{\dagger}(t)\rangle = \frac{1}{L}\int \mathrm{d}A\,\mathrm{Tr}\big(Ae^{-iHt}Ae^{+iHt}\big) \tag{2.20}$$

where $\mathrm{d}A$ is the Haar measure on $U(L)$. Using the mathematical identity $\int \mathrm{d}AA_{jk}A^{\dagger}_{lm} = \frac{1}{L}\delta_{jm}\delta_{lk}$, we obtain

$$\frac{1}{L}\int \mathrm{d}A\langle A(0)A^{\dagger}(t)\rangle = \frac{\mathcal{R}_2^H(t)}{L^2} \tag{2.21}$$

This definition not only provides a link between spectral statistics and 2-point functions, but also provide us a way to calculate the spectral form factor. In a system with large L, instead of integrating over all unitary matrices A, we only need to integrate over some randomly chosen unitary matrices.

Chapter 3

Many-body chaos at weak coupling

This chapter is primarily a reproduction of the paper "Many-body chaos at weak coupling" by Douglas Stanford [6]. The purpose of this reproduction was to get familiar with the methods of calculation in a Quantum Field theory with Matrix Field and apply similar tools in future work.

In the previous chapters, we have looked at some properties and diagnostics of a chaotic system. Here, we will study a large N chaotic system and analytically calculate the largest Lyapunov exponent of the model in the weak coupling regime. We will work with a matrix field of size N in four dimensions in the large N and small 't Hooft coupling($\lambda = g^2 N$) limit. The model is given by the ϕ^4 Lagrangian

$$\mathcal{L} = \frac{1}{2} Tr\left(\dot{\Phi}^2 - (\boldsymbol{\nabla}\Phi)^2 - m^2\Phi^2 - g^2\Phi^4\right) \tag{3.1}$$

We will calculate index averaged and space averaged square commutator given by equation 3.2. The aim of this calculation is to find out the Lyapunov exponent of the model.

$$C(t) = \frac{1}{N^4} \sum_{aba'b'} \int d^3\mathbf{x}\, \mathrm{Tr}\left(\sqrt{\rho}\,[\Phi_{ab}(t,\mathbf{x}), \Phi_{a'b'}]\,\sqrt{\rho}\,[\Phi_{ab}(t,\mathbf{x}), \Phi_{a'b'}]^\dagger\right) \tag{3.2}$$

where the trace is over the system states while the sum on the matrix elements are explicitly specified. In the above commutator, the thermal density matrix has been split into two factors of $\sqrt{\rho}$ to move the operators to opposite sides of thermal circle. This places all the four operators at different space-time points and hence regularizes the

correlation function.

$$\mathrm{Tr}\left(\rho[A(t),B][A(t),B]^\dagger\right) \to \mathrm{Tr}\left(\rho[A(t-i\beta),B(-i\beta)][A(t),B]^\dagger\right) = \mathrm{Tr}\left(\sqrt{\rho}[A(t),B]\sqrt{\rho}[A(t),B]^\dagger\right) \tag{3.3}$$

This regularization should not affect the growth properties, and hence should not change λ_L. We expect that $C(t)$ grows as $e^{2\lambda_L t}$ at large time. To find out λ_L, we will expand the commutators and use Feynman diagram on each term. After expanding the commutator, we can write $C(t)$ diagrammatically as shown in figure 3.1. In the figure, the horizontal axis is the real time, while the verticle axis is the imaginary time with end points identified.

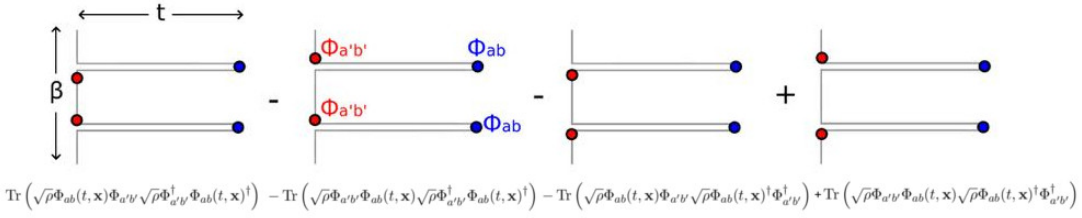

FIGURE 3.1: Diagrammatic representation of terms in $C(t)$

To calculate the Lyapunov exponent, we will employ the following simplifications

1. The N^{-2} term in expansion of $C(t)$ grows as $e^{2\lambda_L t}$, which is also the leading order term in the large N expansion. Therefore, we will be working in large N limit and will only consider planar diagrams.

2. We will restrict integration region only to the real time-fold, i.e. the interaction vertices will be placed only on real time-folds. The interaction over thermal circle should modify the thermal state of the system, but should not affect the growth exponents.

3. Since we want to compute the largest growth exponent, we will only keep the fastest growing terms at each power of λ. As will be shown later, this correspond to summing over only the powers of $\lambda^2 t$ and ignoring the other terms.

Because of these simplifications, the diagrams that must be summed over are the dressed ladder diagrams. There will arise two subtle points in the calculations

1. We are applying perturbation theory on the folded time manifolds, and hence must integrate on both sides of each fold. This summing over the integrals on both sides converts the side rails (horizontal propagator in diagram) into retarded

propagators, while the rungs (propagator between 2 folds) results in Wightman correlators.

2. In the retarded propagator, we need to include self energy correction arising because of propagators lying on the same fold.

The above points will be further clarified in the subsequent sections.

3.1 Free propagators

For the computation of $C(t)$, we will need the retarded propagator G_R and the Wightman correlator G_W defined as follows

$$\begin{aligned}\delta_{ab'}\delta_{ba'}G_R(\mathbf{x},t) &= \theta(t)\,\mathrm{tr}\left(\rho\left[\Phi_{ab}(\mathbf{x},t),\Phi_{a'b'}\right]\right)\\ \delta_{ab'}\delta_{ba'}G_W(\mathbf{x},t) &= \mathrm{tr}\left(\sqrt{\rho}\Phi_{ab}(\mathbf{x},t)\sqrt{\rho}\Phi_{a'b'}\right)\end{aligned} \tag{3.4}$$

At zeroth order in $\lambda = g^2N$, the theory is basically a free field complex Klein-Gordon theory, and the propagators can be calculated directly to give

$$\begin{aligned}G_R(\mathbf{x},t) &= \frac{i}{2E_{\boldsymbol{k}}}\left(\frac{1}{k^0-E_{\boldsymbol{k}}+i\epsilon}-\frac{1}{k^0+E_{\boldsymbol{k}}+i\epsilon}\right)\\ G_W(\mathbf{x},t) &= \frac{\pi}{2E_{\boldsymbol{k}}\sinh\frac{\beta E_{\boldsymbol{k}}}{2}}[\delta(k^0-E_{\boldsymbol{k}})+\delta(k^0+E_{\boldsymbol{k}})]\end{aligned} \tag{3.5}$$

3.2 Order λ^0

At this order, we need to only sum over different ways of contracting the four operators appearing in the figure 3.1. There are three ways to contract the fields as shown in the figure 3.2.

Out of the above cases, the four terms in expansion of B and C adds up to zero, since the contraction does not care about the relative ordering of operators at same imaginary time. Only the case A gives non-zero contribution.

From the figure 3.3, the contribution of diagrams at order λ^0 can be calculated to be

$$\begin{aligned}C(t) &= \frac{1}{N^4}\sum_{a,b,a',b'}\int \mathrm{d}^3x\,\mathrm{Tr}\left(\rho[\Phi_{ab}(\boldsymbol{x},t),\Phi_{a'b'}]\right)\mathrm{Tr}\left(\rho[\Phi^\dagger_{a'b'},\Phi^\dagger_{ab}(\boldsymbol{x},t)]\right)\\ &= -\frac{1}{N^4}\sum_{a,b,a',b'}\int \mathrm{d}^3x\,\mathrm{Tr}\left(\rho[\Phi_{ab}(\boldsymbol{x},t),\Phi_{a'b'}]\right)\mathrm{Tr}\left(\rho[\Phi_{ba}(\boldsymbol{x},t),\Phi_{b'a'}]\right) = -\frac{1}{N^2}\int \mathrm{d}^3x G_R(x,t)^2\end{aligned} \tag{3.6}$$

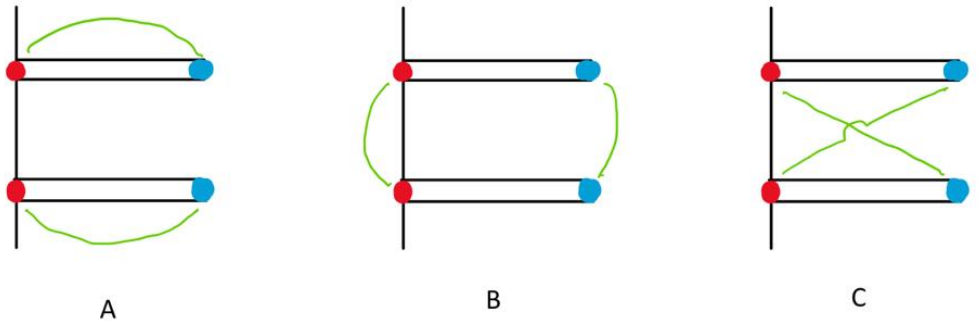

FIGURE 3.2: 3 ways to contract fields at order λ^0

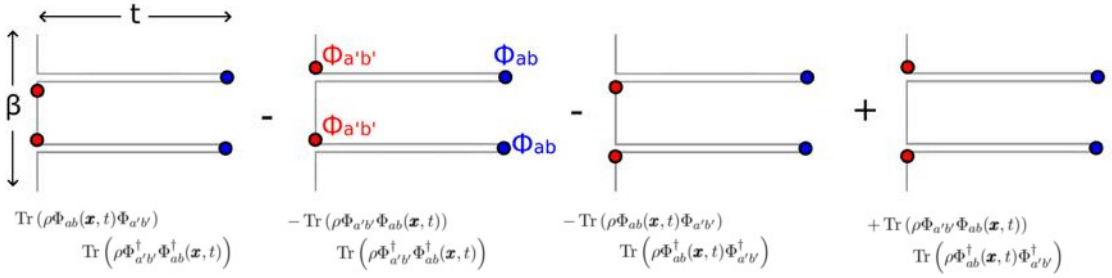

FIGURE 3.3: Terms in expansion of case A

this shows the emergence of the retarded propagator from simple correlators.

3.3 Order λ^1

At order λ, the only possible diagrams are one-loop correction on on the real time folds. These diagrams gives the thermal mass correction to the base mass. This contribution does not modify the Lyapunov at highest order exponent if $m \neq 0$, but contributes to λ_L when $m = 0$

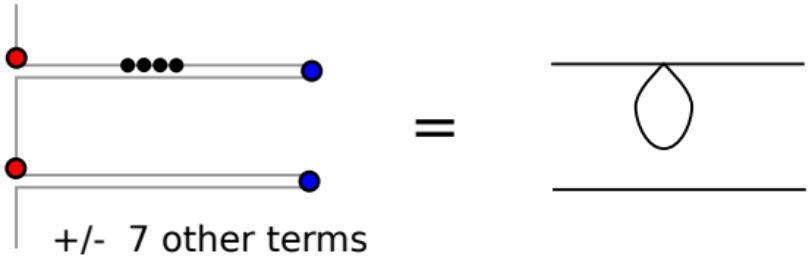

FIGURE 3.4: Diagrams at order λ [6]

We will show in section 3.5 that in the case when bare mass is zero, the one-loop correction generates thermal mass given by $m_{th}^2 = \frac{2\lambda}{3\beta^2}$

3.4 Order λ^2

When we have two integration vertices on the real time fold, we have the following three distinct types of diagrams

1. Two different one-loops (figure 3.5(a) : This correspond to the second term in geometric series generated by one-loop correction. We can ignore this correction in both cases when $m \neq 0$ or when $m = 0$ (relative to thermal mass).

2. Two-loop self energy (figure 3.5(b) : This can also be absorbed as a correction in the propagator according to the Swinger-Dyson equation

$$G(iw_n, (k))^{-1} = G_0(iw_n, (k))^{-1} + \Pi(iw_n, (k))$$

   The real part of the correction Π can be ignored relative to the bare mass or the thermal mass arising out of one-loop correction. The imaginary part of the self energy correction leads to the exponential decay of the correlation function due to scattering. This effect along with higher order dressings of the correlator function can be incorporated by including the imaginary part of the self energy correction in the retarded propagator

$$G_R(\mathbf{x}, t) = \frac{i}{2E_{\boldsymbol{k}}} \left(\frac{1}{k^0 - E_{\boldsymbol{k}} + i\Gamma_{\boldsymbol{k}}} - \frac{1}{k^0 + E_{\boldsymbol{k}} + i\Gamma_{\boldsymbol{k}}} \right) \tag{3.7}$$

   We will not include the effect of self-energy correction in the Wightman correlator because if affects λ_L at a sub-leading order.

3. Rung diagram (figure 3.5(b) : This is a qualitatively new type of diagram when each interaction vertex is attached to different time-fold. This diagram will be analyzed in the section 3.6 in detail.

3.5 Self energy correction

The Schwinger-Dyson equation for incorporating self energy in the propagator is given by

$$G(k)^{-1} = G_0(k)^{-1} + \Pi(k) \tag{3.8}$$

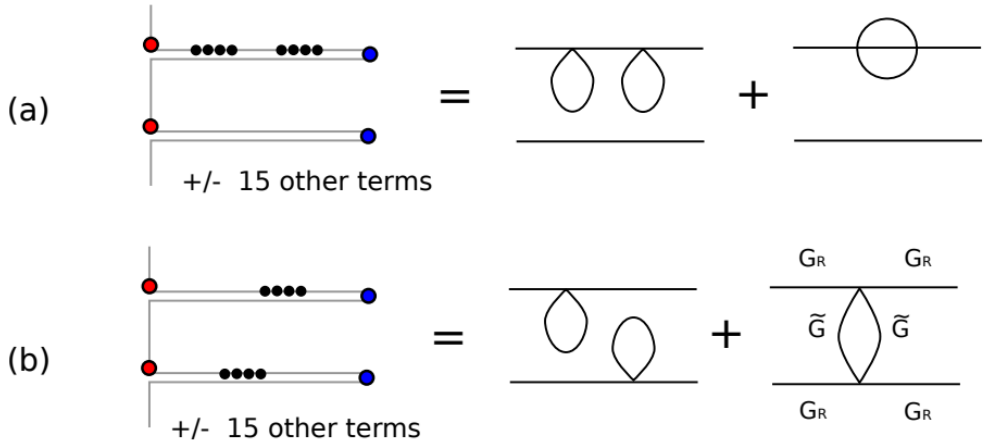

FIGURE 3.5: Diagrams at order λ^2 [6]

where G is the 2-point correlator. Using $G_R(k^0, \mathbf{k}) = -iG(k^0 + i\epsilon, \mathbf{k})$ and under the assumption that Π is small, we can write

$$G_R(k)^{-1} = -i(k^0 + i\Gamma_{\mathbf{k}})^2 + i(E_{\mathbf{k}}^2 + \Sigma_{\mathbf{k}}) \tag{3.9}$$

where we have defined

$$2k^0\Gamma_{\mathbf{k}} = -\operatorname{Im}\{\Pi(k)\} \qquad \Sigma_{\mathbf{k}} = \operatorname{Re}\{\Pi(k)\} \tag{3.10}$$

3.5.1 One-loop self energy

As obvious from the diagram below, the contribution of one-loop free energy does not depend upon the external momenta. The one loop free energy can be obtained by

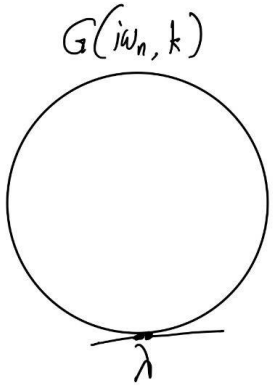

FIGURE 3.6: One loop diagram

summing over the internal momentum at finite temperature in the free propagator shown

in the diagram 3.6. Since, this is only significant in the limit of zero bare mass, we write self energy at $m = 0$ as

$$\Pi = \frac{8\lambda}{\beta} \sum_n \int \frac{d^3\mathbf{p}}{(2\pi)^3} \frac{1}{w_n^2 + \mathbf{p}^2} \tag{3.11}$$

To look at self energy due to temperature T, we subtract the divergent zero temperature contribution from the above integral to get the thermal mass $m_{th}^2 = \frac{2\lambda}{3\beta^2}$.

3.5.2 Two-loop self energy

From the diagram 3.7, we get the two-loop self energy correction

$$\Pi(\tau) = -16\lambda^2 G^3(\tau) \tag{3.12}$$

We are only interested in Imaginary part of the self energy, at $p^0 = E_{\mathbf{p}}$.

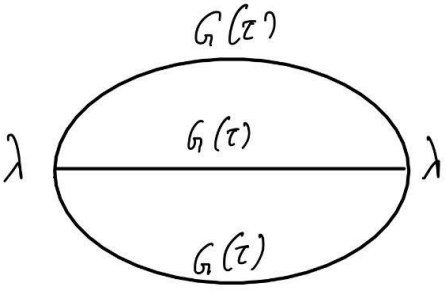

FIGURE 3.7: Two loop diagram

On straightforward evaluation, we can obtain the following expression for $\Gamma_{\mathbf{p}}$

$$\Gamma_{\mathrm{p}} = \frac{\sinh \frac{\beta E_{\mathrm{p}}}{2}}{6E_{\mathrm{p}}} \int \frac{d^4k}{(2\pi)^4} R(p-k)\tilde{G}(k) \tag{3.13}$$

where R is the rung function defined later in equation 3.15.

3.6 Rung Diagram

To evaluate the contribution of diagram 3.5(c), it is beneficial to go to the Fourier space. However, this is troublesome since we expect the function to be exponentially growing, for which the Fourier transform does not exist. Therefore, we will do a Laplace-like transform and define $C(w) = \int_0^\infty \mathrm{d}t e^{iwt} C(t)$. This transformation can be defines by the $i\epsilon$ prescription since the integrand will decay at long times. To recover back $C(t)$, we can simply use Mellin's inverse formula.

In the frequency space, we can directly write the contribution diagram 3.5(c) as

$$C_{rung}(w) = \frac{1}{N^2}\int \frac{\mathrm{d}^4p}{(2\pi)^4}\frac{\mathrm{d}^4q}{(2\pi)^4} G_R(w-p)G_R(p)R(p-q)G_R(w-q)G_R(q) \tag{3.14}$$

where $w-p$ refers to the four momentum $(w-p^0, -p^1, -p^2, -p^3)$. In the above equation, we have defined the Rung Propagator $R(p)$ for later use

$$R(p) = 48\lambda^2 \int \frac{\mathrm{d}^4k}{(2\pi)^4}\widetilde{G}(p/2+k)\widetilde{G}(p/2-k) \tag{3.15}$$

The combinatorial factor of 48 arises since the one-rung diagram has three index structures, and each structure has 16 equivalent diagrams which must be summed over. The explicit evaluation of the Rung function gives the following form, which will be useful for later calculations

$$R(k) = \frac{6\lambda^2}{\pi\beta|\mathbf{k}|\sinh\frac{|k^0|\beta}{2}}\left[\theta\left((k^0)^2-\mathbf{k}^2-4m^2\right)\log\frac{\sinh x_+}{\sinh x_-} + \theta\left(-(k^0)^2+\mathbf{k}^2\right)\log\frac{1-e^{-2x_+}}{1-e^{2x_-}}\right] \tag{3.16}$$

where the variables $x_\pm$ are defined by

$$x_\pm = \frac{\beta}{4}\left(|k^0| \pm |\mathbf{k}|\sqrt{1+\frac{4m^2}{\mathbf{k}^2}-(k^0)^2}\right) \tag{3.17}$$

Since we are only interested in the leading time behavior of $C(t)$, we can further simplify the contribution of one rung diagram. This simplification will also make it evident why we are concerned only with powers of $\lambda^2 t$ in the expansion. In equation 3.14, two pairs of retarded propagators appear and each pair $G_R(w-p)G_R(p)$ is given by

$$-\frac{1}{4E_{\mathbf{p}}^2}\left(\frac{1}{p^0-E_{\mathbf{p}}+i\epsilon}-\frac{1}{p^0+E_{\mathbf{p}}+i\epsilon}\right)\left(\frac{1}{\omega-p^0-E_{\mathbf{p}}+i\epsilon}-\frac{1}{\omega-p^0+E_{\mathbf{p}}+i\epsilon}\right) \tag{3.18}$$

On integration on p^0, we will need to apply the Cauchy integral theorem and will have to take residues at the poles. These residues will generate terms proportional to w^{-1}, $(w+2E_{\mathbf{p}})^{-1}$ and $(w-2E_{\mathbf{p}})^{-1}$. Similar terms will arise when we integrate over the the other pair. Since we know that the fastest growing term in real time correspond to double poles of w in Laplace transform, we make the following change to retain only the terms which give the double pole on integration using Cauchy formula

$$G_R(w-p)G_R(p) \to -\frac{\pi i}{2E_{\mathbf{p}}^2}\frac{\delta(p^0-E_{\mathbf{p}})+\delta(p^0+E_{\mathbf{p}})}{w+2i\epsilon} \tag{3.19}$$

This was done for free propagator. Since the free energy correction occurs only at order λ, we can incorporate the effects of free energy by doing the same modification for

dressed propagators.

$$G_R(w-p)G_R(p) \to -\frac{\pi i}{2E_{\mathbf{p}}^2}\frac{\delta(p^0-E_{\mathbf{p}})+\delta(p^0+E_{\mathbf{p}})}{w+2i\Gamma} \tag{3.20}$$

Because of this substitution, the calculation of $C_{rung}(w)$ will have a double pole at $w=0$. Hence, as specified earlier, the run diagram contributes at order $\lambda^2 t$.

It should be noted that all the Dirac functions appearing in the above expression and in the Wightman functions of the rung propagator forces the integration momenta to be on-shell.

3.7 Building the Ladder

The equation 3.14 can be visualised using the diagram 3.8.

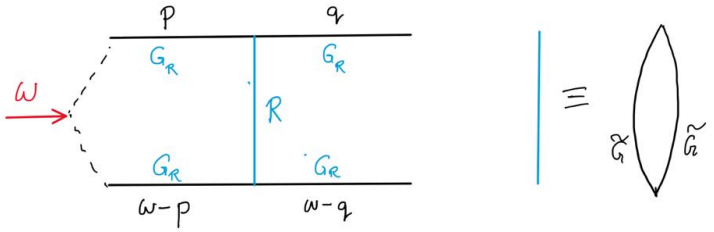

FIGURE 3.8: Diagram corresponding to equation 3.14

In the above diagram, four momentum $w=(w,0,0,0)$ is inserted from left, and we need to integrate over all internal momenta. We need to take care that the horizontal propagators in the diagram are retarded propagators.

At each higher order in λ, the fastest growing contribution will arise from the the additional rung diagram. Any other possible planar diagram at a given order of λ will have lower order of pole, and hence will not contribute to the fastest growing term. In the figure 3.9, the order of λ is 4 while the order of pole at $w=0$ is again 2. This will give subleading contribution of type $\lambda^4 t$.

Now it is evident that rung diagrams will give contribution $(\lambda^2 t)^n$, where n is the number of rungs. For further calculation, we define $f(w,p)$ by the equation

$$C(w)=\frac{1}{N^2}\int\frac{\mathrm{d}^4p}{(2\pi)^4}f(w,p) \tag{3.21}$$

where p is the four-momentum distributed initially between the two side rails.

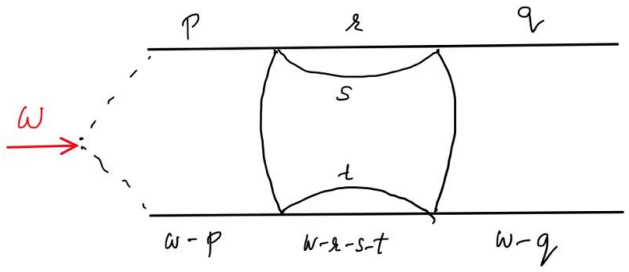

FIGURE 3.9: Diagram not contributing to leading term.

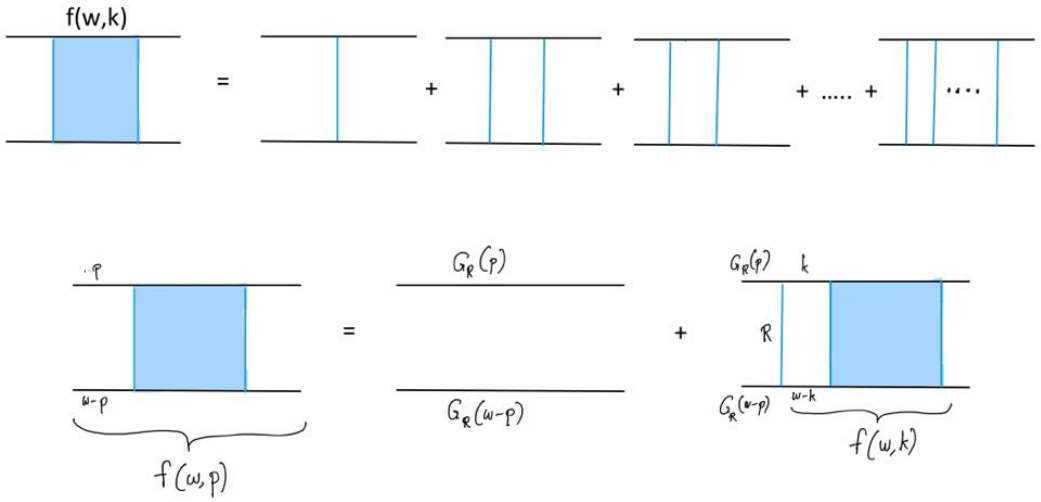

FIGURE 3.10: Ladder Diagrams for $f(w,p)$

As shown in figure 3.10, $f(w,p)$ is sum of infinite terms with increasing number of ladders. We can write the following equation by which must be satisfied by these diagrams

$$f(\omega,p) = -G_R(p)G_R(\omega-p)\left[1+\int \frac{d^4k}{(2\pi)^4}R(k-p)f(\omega,k)\right] \tag{3.22}$$

This is an inhomogeneous equation, and we can find $C(t)$ by first doing an inverse Fourier transform (more accurately, inverse Laplace transform) on the w variable to get $f(t,p)$ and then integrating over the four momentum p. We expect that $f(t,p)$ is an exponentially increasing function at large time. However, the inverse Fourier transform of the first term give a decaying contribution, and hence we can ignore it when attempting to find the growth exponent.

We substitute the form of G_R obtained in equation 3.20 in the expression. This substitution forces the four momentum p to be on shell, which allows us to define h according

to

$$f(w,p) = \delta((p^0)^2 - E_{\mathbf{p}}^2)h(w,\mathbf{p}) \tag{3.23}$$

After substituting approximate expression for G_R and this definition in equation 3.22, we get the following homogeneous equation on integration over k^0

$$-i\omega h(\omega,\mathbf{p}) = -2\Gamma_{\mathbf{p}}h(\omega,\mathbf{p}) + \int \frac{d^3k}{(2\pi)^3}m(\mathbf{k},\mathbf{p})h(\omega,\mathbf{k}) \tag{3.24}$$

where the kernel $m(\mathbf{k},\mathbf{p})$ obtained by integrating over k^0 can be specified in terms of rung function as

$$m(\mathbf{k},\mathbf{p}) = \frac{R\left(k_+\right) + R\left(k_-\right)}{4E_{\mathbf{k}}E_{\mathbf{p}}} \qquad k_\pm = (E_{\mathbf{k}} \pm E_{\mathbf{p}}, \mathbf{k}-\mathbf{p}) \tag{3.25}$$

As claimed before, decay rate Γ influences the growth exponents. Writing the decay rate in terms of the kernel $m(\mathbf{k},\mathbf{p})$, we get the following equation

$$-i\omega h(\omega,\mathbf{p}) = \int \frac{d^3k}{(2\pi)^3}m(\mathbf{k},\mathbf{p})\left(h(\omega,\mathbf{k}) - \frac{\sinh\frac{\beta E_{\mathbf{p}}}{2}}{3\sinh\frac{\beta E_{\mathbf{k}}}{2}}h(\omega,\mathbf{p})\right) \tag{3.26}$$

In the real space, the above equation becomes

$$\frac{d}{dt}h(t,\mathbf{p}) = \sum_{\mathbf{k}} M_{\mathbf{pk}}h(t,\mathbf{k}) \tag{3.27}$$

where M is the integral operator specified above. We can now find λ_L by finding the largest eigenvalue of the matrix M, which can be done numerically.

3.8 Result and Discussion

By solving the equation 3.27, the following results can be obtained

Case	λ_L
$\beta m \ll 1$	$0.025\frac{\lambda^2}{\beta^2 m}$
$\beta m \gg 1$	Decays exponentially with βm
$m = 0$	$0.025\frac{\lambda^2}{\beta^2 m_{th}}$

In the last case when $m = 0$, we need to use the thermal mass arising because of the one-loop correction.

The computation for λ_L was done here only under the limits $\lambda = N^2 g \to 0$ and $N \to \infty$. Therefore, the correction to the λ_L are suppressed by either a factor of λ or by $\frac{1}{N}$.

Chapter 4

Renormalization

Our aim to compute the partition function $\mathcal{Z}(\beta + it)$. We approach this by first calculating the finite temperature partition function $\mathcal{Z}(\beta)$ and then analytically continue this to complex plane. The bare euclidean action is given by

$$S = \frac{1}{2}\int \mathrm{d}^4 x Tr[\partial_\mu \Phi \partial^\mu \Phi + m^2 \Phi^2 + \frac{2g}{4!}\Phi^4] \tag{4.1}$$

We define the *'t Hooft* coupling constant $\lambda = gN$. We will regularize the theory using momentum cut-off and absorb the divergences using appropriate counterterms.

4.1 One Loop Divergence

The bare 2-pt Vertex function (defined as inverse of 2-pt Green's function) is given by

$$\Gamma_B^{(2)} = k^2 + m_B^2 + \frac{\lambda}{3} Q_1(m_B) + \mathcal{O}(\lambda^2) \tag{4.2}$$

where $Q_1(m_B)$ correspond to one-loop correction and is given by

$$Q_1(m_B) = \frac{1}{\beta}\sum_n \int \frac{\mathrm{d}^3 p}{(2\pi)^3} \frac{1}{p^2 + (\frac{2\pi n}{\beta})^2 + m^2} \tag{4.3}$$

Similarly, the lowest order correction is given by the diagrammatic equation

The equation 4.1 results in the follwoing equation

$$\Gamma_B^{(4)} = \frac{\lambda}{6} - \frac{\lambda^2}{36}[L_1(k_1 + k_2, m_B) + L_1(k_1 - k_3, m_B) + L_1(k_1 - k_4, m_B)] \tag{4.4}$$

FIGURE 4.1: 4-pt vertex function

where the function L_1 corresponding to the second diagram in the equation 4.1 is given by

$$L_1(k, w_l, m) = \frac{1}{\beta} \int \frac{\mathrm{d}^3 p}{(2\pi)^3} \left(\frac{1}{p^2 + (\frac{2\pi n}{\beta})^2 + m^2} \right) \left(\frac{1}{(k-p)^2 + (\frac{2\pi(l-n)}{\beta})^2 + m^2} \right) \tag{4.5}$$

From the 2-pt vertex function and the 4-pt vertex function, we can obtain the first order correction to bare mass and bare coupling constant

$$m_1^2 = m_B^2 + \frac{\lambda}{3} Q_1(m_B) \tag{4.6}$$

$$\lambda_1 = \lambda - \frac{\lambda}{2} L_1(0, m_B) \tag{4.7}$$

4.2 Two Loop Divergence

We can find the two loop correction to the 2-pt function using the following diagrammatic equation

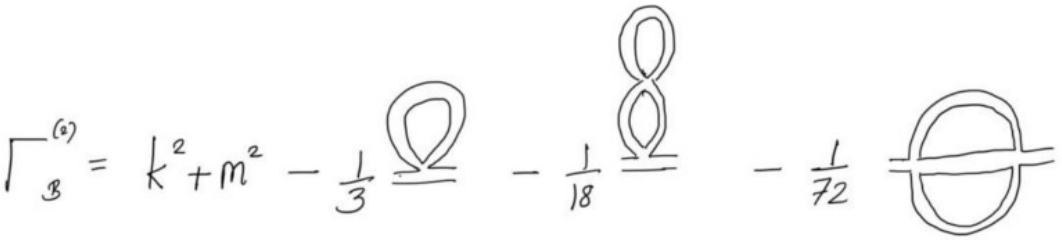

FIGURE 4.2: 2-pt vertex function

which translate in the equation

$$\Gamma_B^{(2)} = \frac{1}{\beta} \sum_n \int \frac{\mathrm{d}^3 p}{(2\pi)^3} \frac{1}{p^2 + (\frac{2\pi n}{\beta})^2 + m^2} - \frac{\lambda^2}{18} Q_2(m_B) Q_1(m_B) - \frac{\lambda^2}{72} Q_3(k, m_B) \tag{4.8}$$

where the functions Q_2 and Q_3 are given by

$$Q_2(m_B) = \frac{1}{\beta}\sum_n \int \frac{\mathrm{d}^3p}{(2\pi)^3}\left(\frac{1}{p^2+(\frac{2\pi n}{\beta})^2+m^2}\right)^2 \tag{4.9}$$

$$Q_3(k,w_l,m_B) = \frac{1}{\beta}\sum_{n_1,n_2}\int \frac{\mathrm{d}^3p_1}{(2\pi)^3}\frac{\mathrm{d}^3p_2}{(2\pi)^3}\left(\frac{1}{p_1^2+(\frac{2\pi n_1}{\beta})^2+m^2}\right)\left(\frac{1}{p_2^2+(\frac{2\pi n_2}{\beta})^2+m^2}\right) \left(\frac{1}{(k-p_1-p_2)^2+(\frac{2\pi(l-n_1-n_2)}{\beta})^2+m^2}\right) \tag{4.10}$$

The integral in Q_3 seems very difficult to evaluate, and we will only concern ourselves to first order in λ for now.

4.3 Partition Function

Writing the action only till first order in λ

$$S = \frac{1}{2}\int \mathrm{d}^4x Tr[\partial_\mu\Phi\partial^\mu\Phi + (m_1^2 - \frac{2\lambda}{3}Q_1(m_1))\Phi^2 + \frac{\lambda}{4!*N}\Phi^4] \tag{4.11}$$

Let us first define the partition function for the scalar free field

$$\mathcal{Z}_{1f}(\beta,m) = \int \mathcal{D}\phi \exp\left\{-\frac{1}{2}\int \mathrm{d}^4x \partial_\mu\phi\partial^\mu\phi + m^2\phi^2\right\} \tag{4.12}$$

We can directly canculate this partition function to give

$$\ln \mathcal{Z}_{1f} = V\int \frac{\mathrm{d}^3p}{(2\pi)^3}\left(-\frac{1}{2}\beta w_p - \ln\left(1-e^{-\beta w_p}\right)\right) \tag{4.13}$$

The first term is divergent, but since it correspond to zero point energy, it has no physical significance. It can be removed by adding an appropriate constant counter term to the lagrangian. The integral of the second term is finite.

Observing that there are N^2 fields in out original lagrangian, we write the partition function

$$\ln \mathcal{Z} = N^2 \ln \mathcal{Z}_{1f} + \left(\frac{\lambda}{6}\int \mathrm{d}^x Q_1\langle\Phi_{ab}\Phi_{ba}\rangle - \frac{\lambda}{48}\int \mathrm{d}^x\langle\Phi_{ab}\Phi_{bc}\Phi_{cd}\Phi_{da}\rangle\right) \tag{4.14}$$

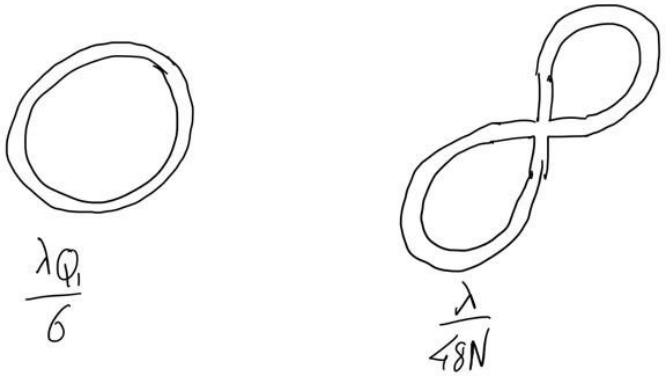

FIGURE 4.3: Vacuum diagram at order λ

The expectation values can be evaluation using the following two diagrams

Evaluating the diagrams in figure 4.3 give the following equation

$$\ln \mathcal{Z} = N^2 \ln \mathcal{Z}_{1f} + \lambda N^2 \beta V \left(\frac{1}{6} Q_1(m_B) G(r=0) - \frac{1}{24} G^2(r=0) \right) \tag{4.15}$$

We observe that the $Q_1(m_B) = G(r=0)$ and both are given by

$$G(r=0) = \frac{1}{\beta} \sum_n \int \frac{\mathrm{d}^3 p}{(2\pi)^3} \frac{1}{p^2 + (\frac{2\pi n}{\beta})^2 + m^2} \tag{4.16}$$

This reduces the final partition function to

$$\ln \mathcal{Z} = N^2 \ln \mathcal{Z}_{1f} + \frac{\lambda N^2 \beta V}{8} G^2(r=0) \tag{4.17}$$

However, even after renormalization, the fourier transform of green's function is Not finite. I am unable to procees beyond this point.

In the reference https://www.imperial.ac.uk/media/imperial-college/research-centres-and-groups/theoretical-physics/msc/dissertations/2011/Yuhao-Yang-Dissertation.pdf in section 3.2.4 , the author simply ignores the divergent part coming because of zero temperature contribution and only include the finite part in $G(r=0)$. I do not think this is justified as no renormaliztion procedure is applied.

We can further analyze the Greens function as $r = 0$.

$$G(r=0) = \frac{1}{\beta}\sum_n \int \frac{\mathrm{d}^3p}{(2\pi)^3}\frac{1}{p^2 + (\frac{2\pi n}{\beta})^2 + m^2} = \int \frac{\mathrm{d}^3p}{(2\pi)^3}\frac{\coth\frac{\beta w_p}{2}}{2w_p}$$
$$= \int \frac{\mathrm{d}^3p}{(2\pi)^3}\frac{\coth\frac{\beta w_p}{2} - 1}{2w_p} + \int \frac{\mathrm{d}^3p}{(2\pi)^3}\frac{1}{2w_p} \quad (4.18)$$

In the above equation, the first part is finite temperature dependent part while the second term is the divergence due to $T = 0$ contribution. However, it seems difficult to remove the divergent part from the squared propagator appearing in the partition function.

Chapter 5

Renormalization-2

In this chapter, I will renormalize the action upto two loop order using the method from the article here: https://cds.cern.ch/record/290497/files/9510232.pdf.

Once again, the action is given by

$$\ln \mathcal{Z} = N^2 \ln \mathcal{Z}_{1f} + \left(\frac{\lambda}{6} \int \mathrm{d}^x Q_1 \langle \Phi_{ab} \Phi_{ba} \rangle - \frac{\lambda}{48} \int \mathrm{d}^x \langle \Phi_{ab} \Phi_{bc} \Phi_{cd} \Phi_{da} \rangle \right) \tag{5.1}$$

the corresponding greens function are

$$G_0(k) = \langle \Phi_{ab} \Phi_{ba} \rangle = \frac{1}{p^2 + m^2} \tag{5.2}$$

We represent the free energy upto order λ^2 as

$$\frac{f}{N^2} = -\frac{\ln Z}{\beta V} = f^{(1)}(T) + f^{(2)}(T) + f^{(3)}(T) \tag{5.3}$$

While doing the renormalization calculation, we will be separating the thermal fluctuations and vacuum fluctuations. The vacuum fluctuations can be obtained from the thermal fluctuations by taking the limit $T \to 0$.

$$\frac{1}{\beta} \sum_{p_0} \to \frac{1}{2\pi} \int_{-\infty}^{\infty} \mathrm{d}p_0 \tag{5.4}$$

The summation over p_0 is actually over the bosonic Matsubara frequency.

5.1 Setting up Diagrams

We will now set up diagrammatic representation for carrying out the calculations in rest of the chapter.

The elementary loop (which will be later related to energy of free field) is given by

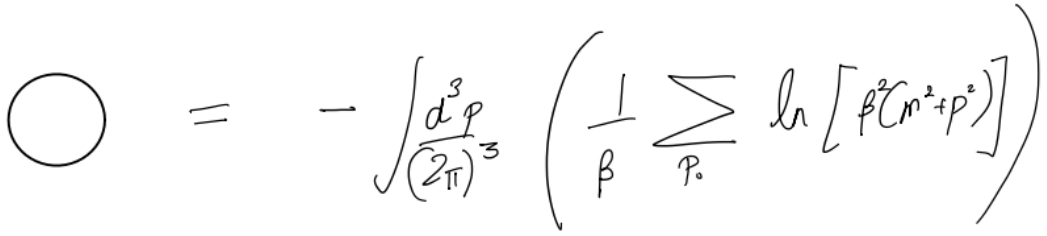

FIGURE 5.1: Elementary Loop

On evaluating the loop, we obtain

$$\bigcirc = \frac{-2}{\beta} \int \frac{d^3p}{(2\pi)^3} \ln\left(1 - e^{-\beta\omega}\right) + a + bT \tag{5.5}$$

where a, b are divergent quantities which are irrelevant since they can be removed simply by adding constant to Lagrangian or normalizing the action. Also, these quantities correspond to terms in partition function $\mathcal{Z}(\beta + it)$ which has no time-dependence, and hence does not affect time evolution of Spectral form factor.

We call the convergent part in above expression as thermal contribution and the divergent part as vacuum contribution. This gives

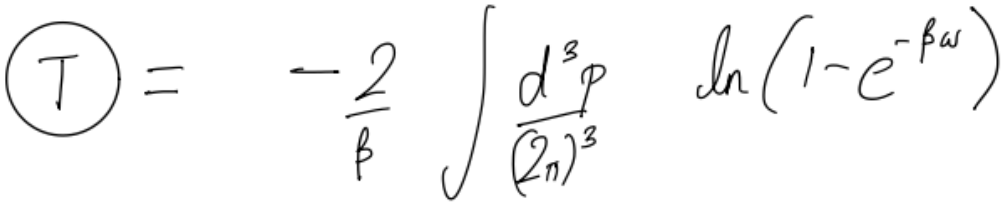

FIGURE 5.2: Thermal part of Elementary Loop

We define the following diagram useful for calculating corrections to free-field free The

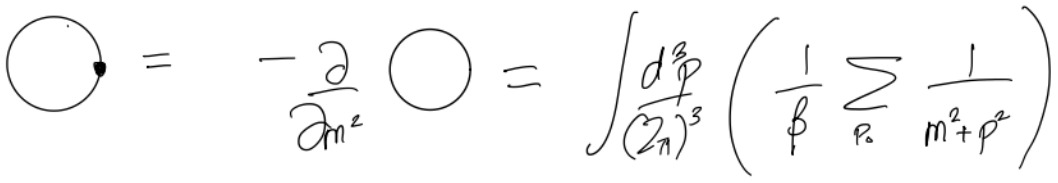

FIGURE 5.3: derivative diagram

above diagram again breaks into sum of thermal contribution and vacuum contribution

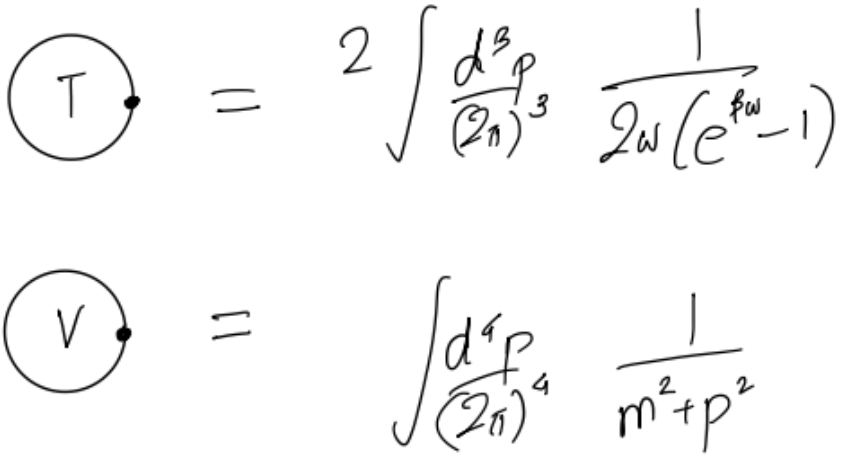

FIGURE 5.4: contributions to derivative diagram

Observe that the thermal diagram has a Bose-Einstein statistical factor. More complex diagram has more number of these statistical factors, and we will use these to classify the diagrams.

Once again, we can take the derivative of the previous diagram to get the following

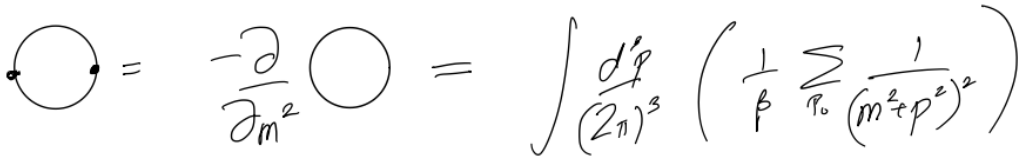

FIGURE 5.5: second-derivative diagram

Again, the above diagram can be expressed as sum of thermal part and vacuum part.

We will join these elementary diagrams to obtain diagrams corresponding to corrections to free energy. Since we are only looking upto second order in perturbation theory, it is enough to use diagrams with just two vertices (derivatives). Let us look at some useful composite diagrams

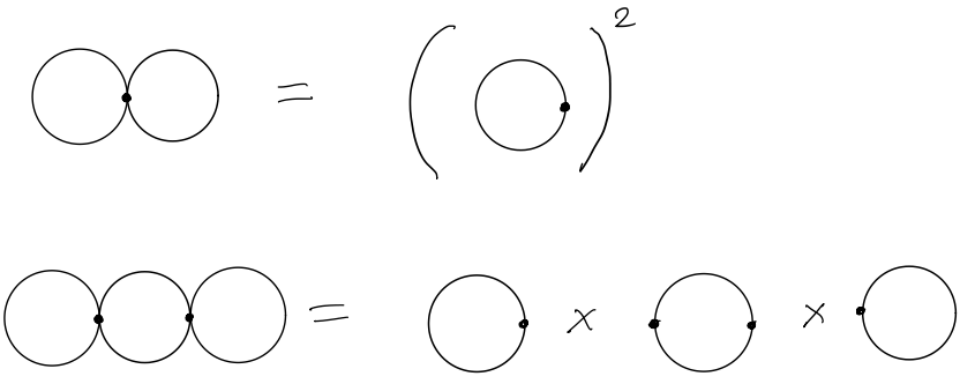

FIGURE 5.6: Composite diagrams

Apart from the above composite diagrams, we will need two additional diagrams for representation.

The first one is not a vacuum diagram, but actually one of the diagram contributing the self-energy. It is the two-loop contribution, such that the external propagator is on the mass shell.

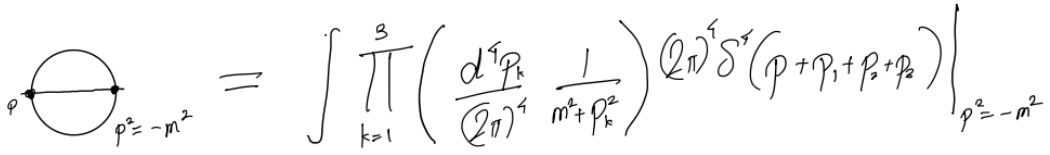

FIGURE 5.7: Two-loop contribution to self energy

The other diagram that is important is the following one

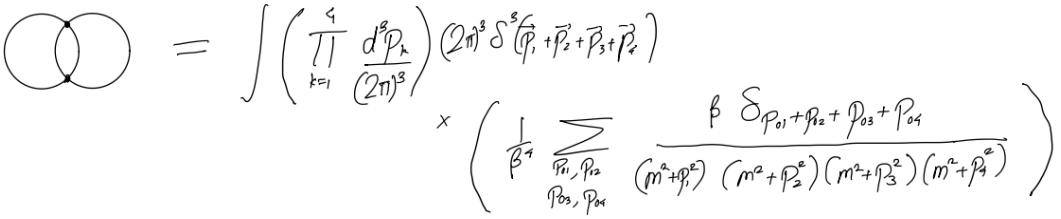

FIGURE 5.8: Second order correction

The above diagram can be represented as sum of diagrams with increasing number of thermal loop. Each thermal loop contribute the Bose-Einstein statistical factor. The combinatorial factors are arranged according to the number of ways we can cut 0,1,2 or 3 lines in the diagram.

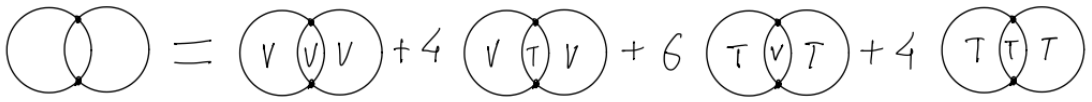

FIGURE 5.9: Contributions to the diagram for second order correction

We can explicitly calculate the integral in above diagrammatic expression to obtain

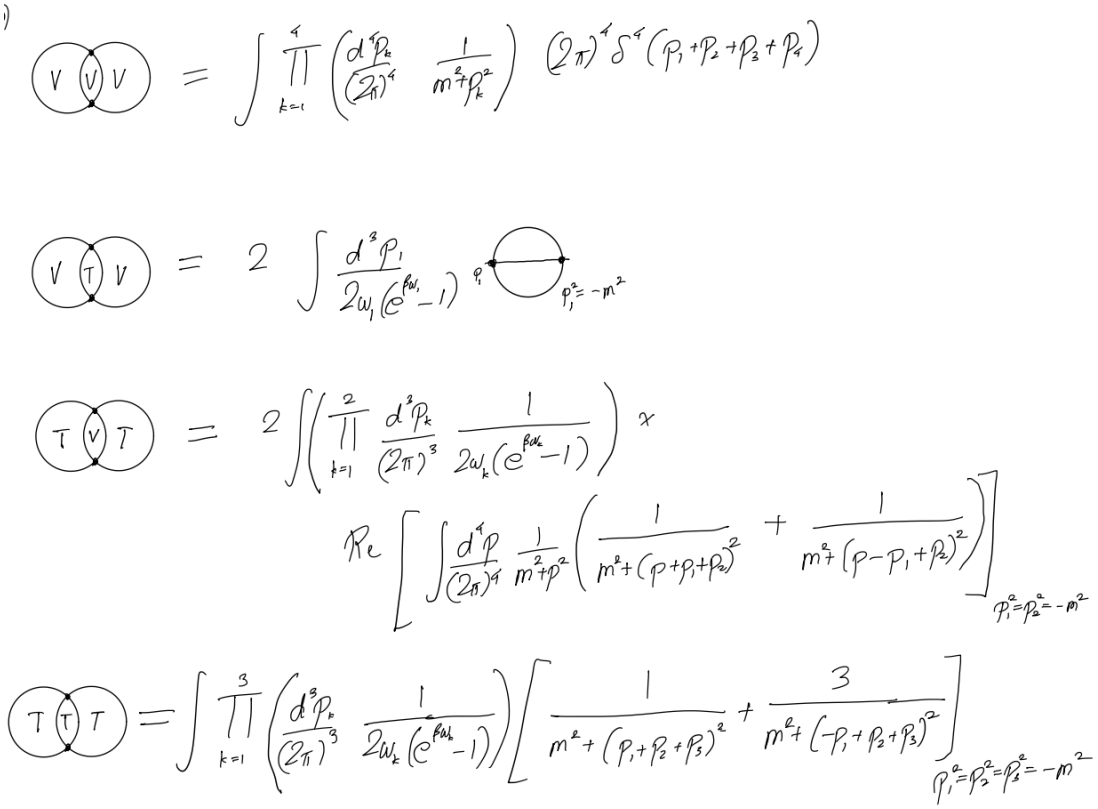

FIGURE 5.10: Expressions for Contributions to the diagram for second order correction

5.2 Free energy

Let us write the contribution to free energy by only using the bare action

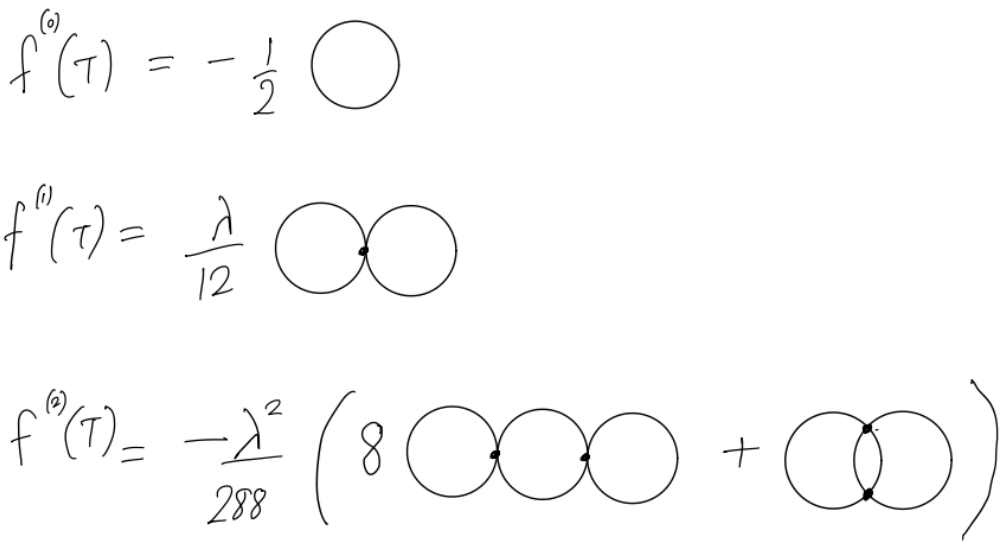

FIGURE 5.11: Free Energy from bare action

5.3 Renormalization

5.3.1 First order correction

At first order, it suffices to just shift the mass.

$$m^2 \to m^2 - \delta m_1^2 \tag{5.6}$$

Using the equation ??, we see that the above modification changes corrects the elementary diagram according to

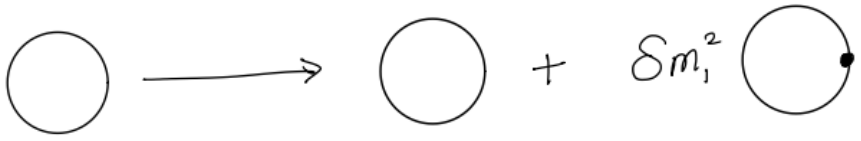

FIGURE 5.12: Correction to elementary diagram

Hence, upto first order in λ, the free energy is given by

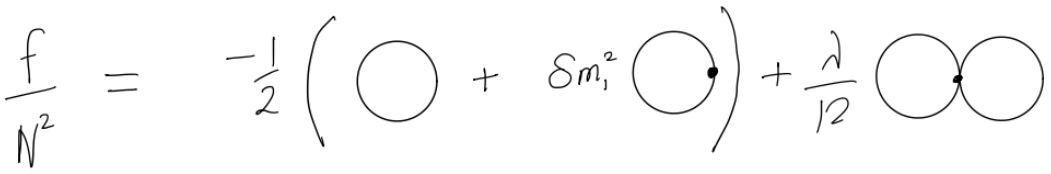

FIGURE 5.13: corrected free energy upto first order

To renormalize, we need to remove the contribution in $f^{(2)}$ with one thermal loop and one vacuum loop, and hence

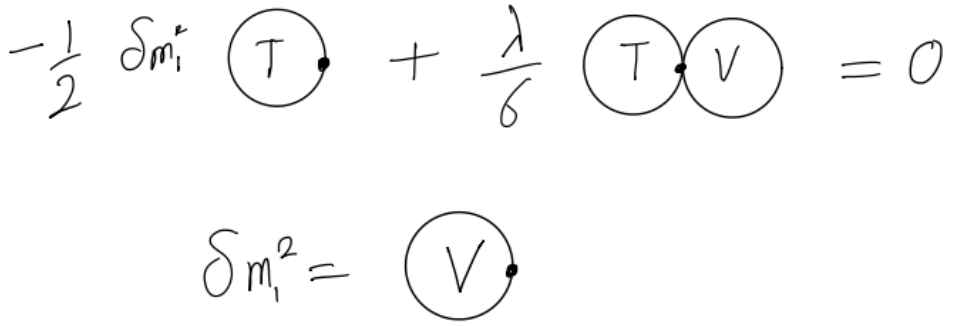

FIGURE 5.14: First order counter term

Substituting this value and ignoring the diagrams corresponding to $T = 0$, we get the renormalized free energy upto first order as

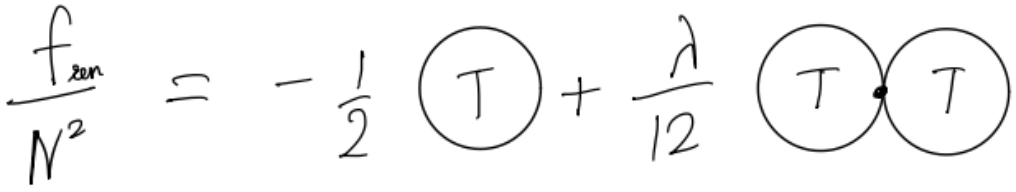

FIGURE 5.15: renormalized Free energy upto first order

5.3.2 Second order correction

To correct the free energy at second order, we make the following modification

$$m^2 \to m^2 - \delta m_1^2 - \delta m_2^2 \quad , \quad \lambda \to \lambda - \delta\lambda \tag{5.7}$$

We additionally make the following substitution for convenience

$$\delta m_2^2 = a_2\lambda^2 \qquad , \qquad \delta\lambda = a_1\lambda^2 \tag{5.8}$$

These substitution makes the following modification in the free energies

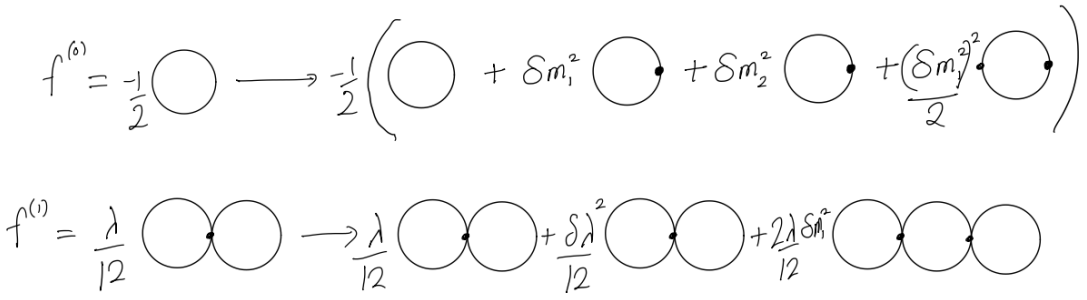

FIGURE 5.16: modification to first order free energy

Absorbing the second order correction into $f^{(2)}$, we get the following modification

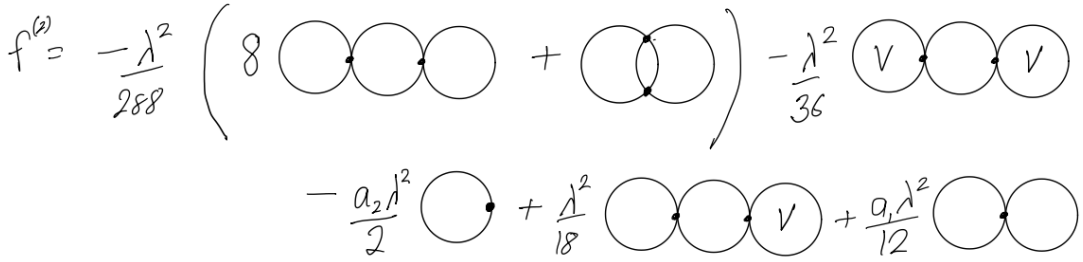

FIGURE 5.17: Free energy second order modification

Now our aim is to choose the values of a_1, a_2 such that the only divergences that occur are due to $T = 0$ diagrams. For this, we proceed by renormalizing diagrams at each T-loop order.

5.3.2.1 3 T-loops

This is given by the following expression, which is finite

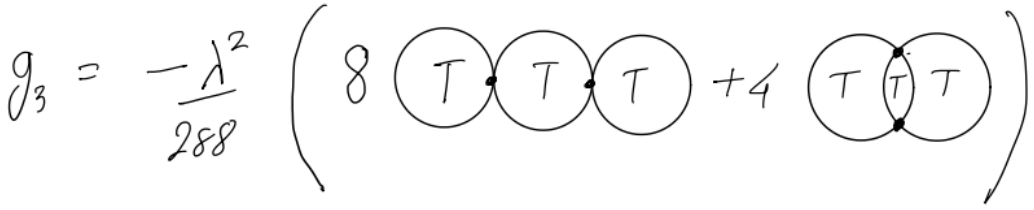

FIGURE 5.18: 3 T-loops

5.3.2.2 2 T-loops

The 2-T loop contributions are given by

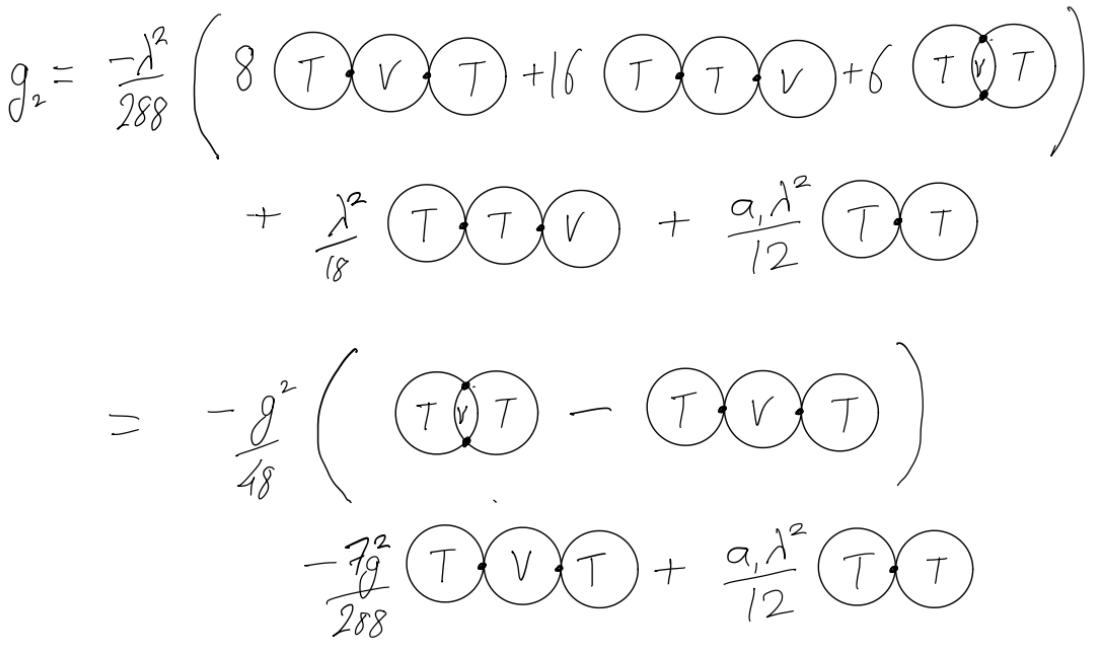

FIGURE 5.19: 2 T-loops

The term inside the bracket is finite and is given by

$$\left(\cdots \right) = \frac{2}{(2\pi)^6} \int \frac{d^3\mathbf{p}_1 d^3\mathbf{p}_2}{2\omega_1 2\omega_2 \left(e^{\beta\omega_1}-1\right)\left(e^{\beta\omega_2}-1\right)} \times$$
$$\times \mathbf{Re}\left[\frac{1}{(2\pi)^4} \int \frac{d^4p}{m^2+p^2} \left(\frac{1}{m^2+(p+p_1+p_2)^2} + \frac{1}{m^2+(p-p_1+p_2)^2} - \frac{2}{m^2+p^2} \right) \right]$$

To cancel the divergent term, we need

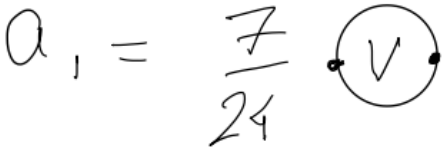

FIGURE 5.20: a_1 value

Hence, the renormalized 2 T-loop contribution is given by

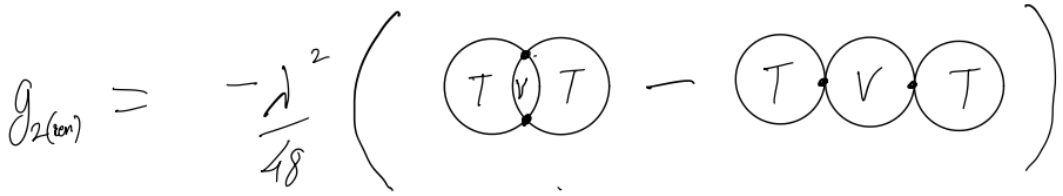

FIGURE 5.21: renormalized 2 T-loops contribution

5.3.2.3 1 T-loops

The 1 T-loop correction is given by

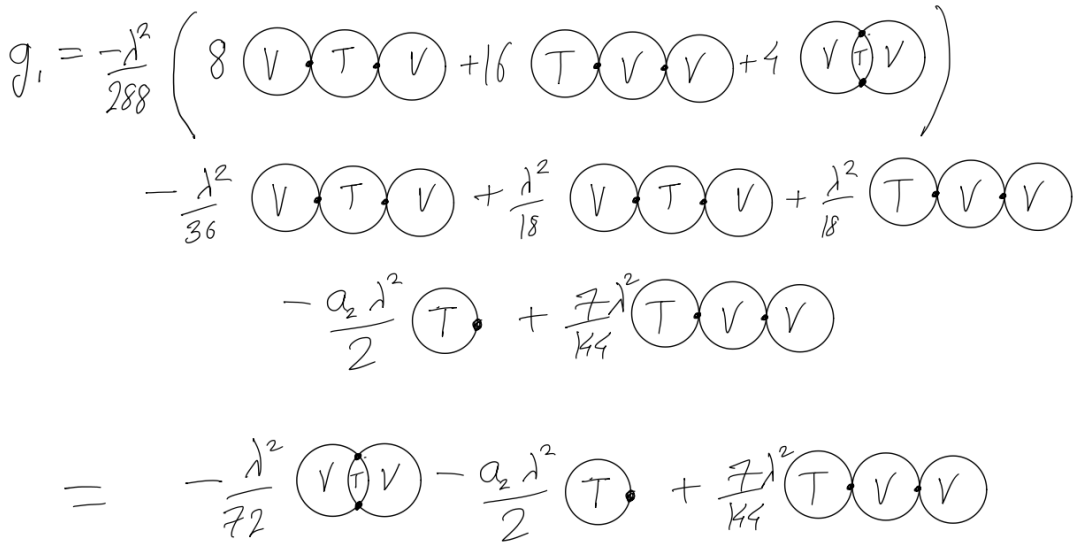

FIGURE 5.22: 1 T-loops

We see that g_1 is 0 if we choose a_2 according to

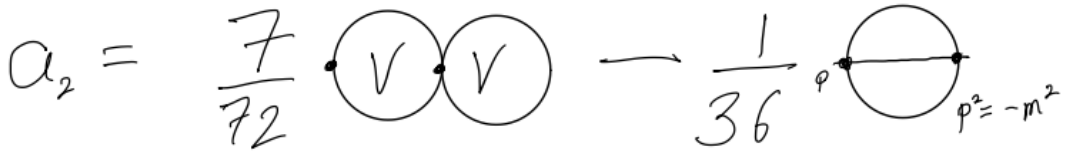

FIGURE 5.23: a_2 value

5.4 Renormalized Free Energy

We add up all the renormalized terms back to get the renormalized free energy with no vacuum contribution as

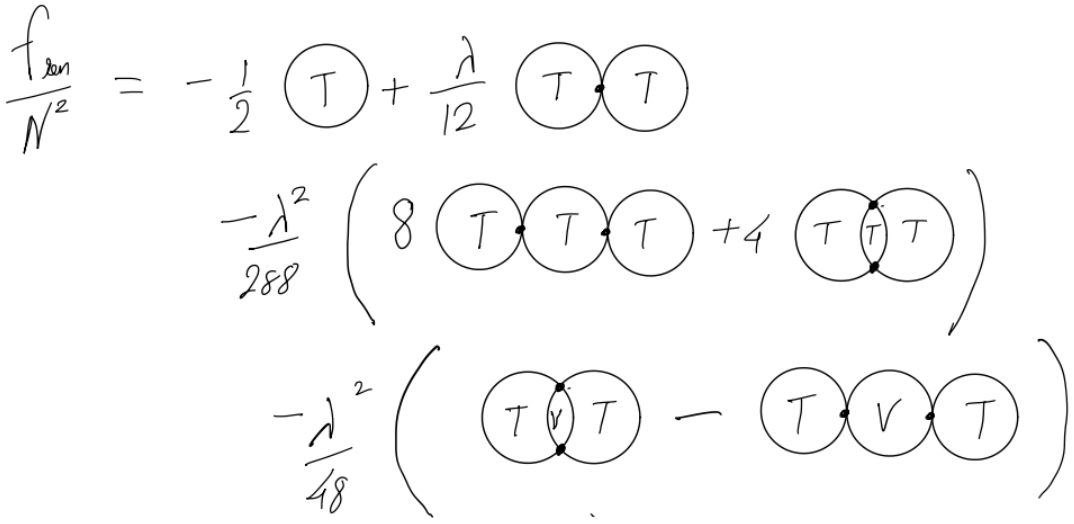

FIGURE 5.24: Renormalized Free Energy

Bibliography

[1] Juan Maldacena, Stephen H. Shenker, and Douglas Stanford. A bound on chaos. *Journal of High Energy Physics*, 2016(8):106, Aug 2016.

[2] Viktor Jahnke. Recent developments in the holographic description of quantum chaos. 2018.

[3] Jordan S. Cotler, Guy Gur-Ari, Masanori Hanada, Joseph Polchinski, Phil Saad, Stephen H. Shenker, Douglas Stanford, Alexandre Streicher, and Masaki Tezuka. Black holes and random matrices. *Journal of High Energy Physics*, 2017(5), May 2017.

[4] Jordan Cotler, Nicholas Hunter-Jones, Junyu Liu, and Beni Yoshida. Chaos, complexity, and random matrices. *Journal of High Energy Physics*, 2017(11), Nov 2017.

[5] Junyu Liu. Spectral form factors and late time quantum chaos. *Physical Review D*, 98(8), Oct 2018.

[6] Douglas Stanford. Many-body chaos at weak coupling. *Journal of High Energy Physics*, 2016(10), Oct 2016.